Inorganic Chemistry

Article

pubs.acs.org/IC

Electronic Structures of the $[V(^{t}bpy)_3]^z$ (z = 3+, 2+, 0, 1−) Electron Transfer Series

Amanda C. Bowman,[†,‡] Stephen Sproules,*[,†,§] and Karl Wieghardt*[,†]

[†]Max-Planck-Institut für Bioanorganische Chemie, Stiftstrasse 34-36, D-45470 Mülheim an der Ruhr, Germany

[§]EPSRC National UK EPR Facility and Service, Photon Science Institute, The University of Manchester, Oxford Road, Manchester M13 9PL, U.K.

Supporting Information

ABSTRACT: The electron transfer series of complexes $[V(^{t}bpy)_3]^z$ (z = 3+, 2+, 0, 1−) has been synthesized and spectroscopically characterized with the exception of the monocationic species. Magnetic susceptibility measurements (4−290 K) establish an S = 1 ground state for $[V(^{t}bpy)_3]^{3+}$, $S = {}^3/_2$ for $[V(^{t}bpy)_3]^{2+}$, $S = {}^1/_2$ for $[V(^{t}bpy)_3]$, and an S = 0 ground state for $[V(^{t}bpy)_3]^{1-}$. The electrochemistry of this series recorded in tetrahydrofuran solution exhibits four reversible one-electron transfer steps. Electronic absorption, X-band electron paramagnetic resonance (EPR), and V K-edge X-ray absorption (XAS) spectra were recorded. All complexes have been studied computationally with density functional theory (DFT) using the B3LYP functional. It is unequivocally shown that the electronic structure of complexes is best described as $[V^{III}(^{t}bpy^0)_3]^{3+}$, $[V^{II}(^{t}bpy^0)_3]^{2+}$, $[V^{II}(^{t}bpy^{\bullet})_2(^{t}bpy^0)]^0$, and $[V^{II}(^{t}bpy^{\bullet})_3]^{1-}$, where $(^{t}bpy^0)$ represents the neutral form of the ligand and $(^{t}bpy^{\bullet})^{1-}$ is the one-electron reduced mononanionic radical form. In the neutral and monoanionic members, containing two and three $(^{t}bpy^{\bullet})^{1-}$ ligands, respectively, the ligand spins are strongly antiferromagnetically coupled to the spins of the central V(II) ion (d^3; $S = {}^3/_2$) affording the observed ground states given above.

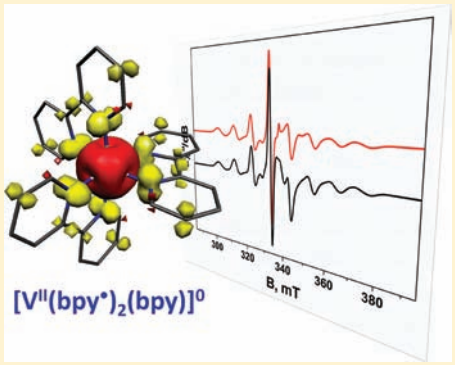

INTRODUCTION

It is now well established that the most commonly used *N*-heterocyclic ligand 2,2′-bipyridine (bpy) is redox-active and can exist in coordination compounds as either a neutral bidentate ligand (bpy^0), a π radical anion, $(bpy^{\bullet})^{1-}$, or a diamagnetic dianion $(bpy^{2-})^{2-}$ (Scheme 1).[1,2] Quite remarkably, many homoleptic tris(bipyridine) neutral complexes of the transition metal ions have been shown to be a member of an electron transfer series, for example, $[M(bpy)_3]^z$, where z may vary from 3+ to 3− in single electron steps.[2] For chromium, seven(!) such species have been isolated as solids.[3,4] We have recently shown that all of these species contain a central Cr(III) ion (d^3), and the reversible one-electron oxidations and reductions are all ligand-based processes.[2] The ligand mixed-valency species $[Cr^{III}(bpy^{\bullet})(bpy^0)_2]^{2+}$ was shown to be localized (class II).

It is interesting that for the corresponding vanadium complexes a similar electron transfer series appears to exist, $[V(bpy)_3]^z$ (z = 3+, 2+, 1+, 0, 1−, 2−, 3−).[5] Salts of the tri- and dication and of the (impure) monocation as well as the neutral and the monoanion have all been described in the literature:[6] $[V(bpy)_3]^z$ (z = 3+, 2+, (1+), 0, 1−). Thus, the first two species have been described as $[V^{III}(bpy^0)_3]^{3+}$ (S = 1) and $[V^{II}(bpy^0)_3]^{2+}$ ($S = {}^3/_2$), respectively. For the neutral species, varying electronic structures have been uncovered in the literature such as $[V^0(bpy^0)_3]$ containing a central low-spin V d^5 atom bound by three neutral (bpy^0) ligands[6,7] or $[V^{III}(bpy^{\bullet})_3]$ bearing a V(III) d^2 ion coordinated by three π radical monoanions.[8] The overall $S = {}^1/_2$ ground state is proposed to be attained via strong antiferromagnetic coupling. Note that in the first description the unpaired electron resides in a d orbital, whereas it is in a single $(bpy^{\bullet})^{1-}$ ligand in the latter. Surprisingly, both formulations have been proposed based on the same experimental EPR spectrum.[7−11]

For the monoanion $[V(bpy)_3]^{1-}$ (S = 0),[6] no specific electronic structure has been put forward except that some electron density is expected on the ligands. The compound $Na_3[V(bpy)_3]\cdot 7THF$ containing a tris(bipyridine)vanadium trianion and possessing an S = 1 ground state has also been reported.[12] In the light of our present work it is conceivable that this species contains a central V(II) d^3 ion with two diamagnetic (bpy^{2-}) dianions and one $(bpy^{\bullet})^{1-}$ π radical anion: $[V^{II}(bpy^{2-})_2(bpy^{\bullet})]^{3-}$. The S = 1 ground state is realized through antiferromagnetic coupling of the ligand radical with the central metal ion.

Here we have synthesized a new series of such vanadium complexes containing the substituted ligand 4,4′-di-*tert*-butyl-2,2′-bipyridine (^{t}bpy): $Na[V(^{t}bpy)_3]$ (S = 0), $[V(^{t}bpy)_3]$ ($S = {}^1/_2$), $[V(^{t}bpy)_3](BF_4)_2$ ($S = {}^3/_2$), $[V(^{t}bpy)_3](BF_4)_3$ (S = 1). It has not been possible to include $[V(^{t}bpy)_3](BF_4)$ (S = 1) in pure form because of its rapid disproportionation in solution to a mixture of the neutral and dicationic species.[6] The reason for

Received: December 17, 2011
Published: March 6, 2012

Scheme 1

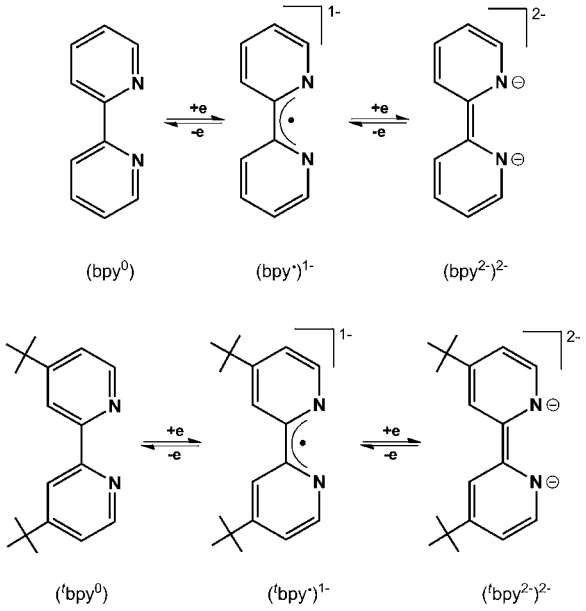

choosing the ^{t}bpy ligand in contrast to unsubstituted bpy was the observation that in the corresponding suite of chromium complexes, diffraction quality crystals were obtained where the site symmetry of the respective central chromium ion did not involve a threefold axis rendering the three ^{t}bpy ligands equivalent in the solid state for crystallographic reasons.[2] This was in contrast to the corresponding crystal structures of salts of the tri-, di-, and monocations of the $[Cr(bpy)_3]^z$ series which all displayed C_3 symmetry with accompanying static disorder problems of the bpy ligands for the di- and monocations.[13,14]

Surprisingly, from the $[V(bpy)_3]^z$ (z = 3+, 2+, 1+, 0) series only the neutral complex has been targeted by X-ray crystallography.[13] The low quality of this 1963 structure determination only allows for the atom connectivity to be unequivocally established for the octahedral VN_6 polyhedron. All other members have not been structurally characterized to date. Disappointingly, we have not managed to alter this position in many attempts to grow single crystals of our synthesized series. Nonetheless, the electronic structures have been elucidated using a combination of XAS, electronic, and EPR spectroscopy, as well as magneto- and electrochemistry. The experimental data are interpreted in concert with density functional theoretical (DFT) calculations to clearly define the location of valence electrons in these multiredox-centered coordination compounds.

EXPERIMENTAL SECTION

Syntheses. All air- and moisture-sensitive manipulations were carried out under a purified argon atmosphere using standard Schlenk techniques or glovebox. Solvents were dried and deoxygenated according to literature procedures.[15] VCl_3 and sodium amalgam beads (5%) were purchased from Sigma Aldrich and used as received. Tropylium tetrafluoroborate, ferrocenium tetrafluoroborate, and 4,4′-di-*tert*-butyl-2,2′-bipyridine (^{t}bpy) were purchased from Sigma Aldrich and dried in vacuo before use. Naphthalene was purchased from Sigma Aldrich and sublimed before use.

Na[V(^{t}bpy)$_3$]·3THF. A 50 mL round-bottom flask was charged with Na (6 mg; 0.26 mmol) and naphthalene (33 mg; 0.21 mmol) in THF (25 mL). The solution was stirred for several hours until bright green in color and the sodium metal was no longer visible. To this solution was added [V(^{t}bpy)$_3$] (200 mg; 0.23 mmol), and the reaction was stirred for an additional 2 h, after which time volatiles were removed to yield a dark brown powder. The powder was washed with toluene to remove naphthalene and recrystallized from THF at −35 °C to give a dark brown microcrystalline solid. Yield: 220 mg (85%).

[V(^{t}bpy)$_3$]. A mixture of VCl_3 (0.19 g; 1.21 mmol) and ^{t}bpy (1.00 g; 3.73 mmol) in THF (25 mL) was treated with Na amalgam (5 wt. %; 1.94 g; 4.22 mmol) and stirred at ambient temperature for 18 h wherein the color became deep blue. The solution was filtered through Celite, and volatiles were removed under vacuum. The residue was recrystallized from THF/diethyl ether at −35 °C giving a dark blue microcrystalline solid. Yield: 0.750 g (73%).

[V(^{t}bpy)$_3$](BF$_4$)$_2$. A 20 mL scintillation vial containing [V(^{t}bpy)$_3$] (150 mg; 0.18 mmol) dissolved in THF (15 mL) was treated portionwise with tropylium tetrafluoroborate (62 mg; 0.35 mmol). The reaction mixture was stirred for 6 h giving a bright blue-green solution. The solution was concentrated under vacuum and cooled to −35 °C, affording a dark green precipitate. This was collected on a frit, washed with toluene, and recrystallized from acetonitrile/diethyl ether. Yield: 160 mg (91%).

Anal. Calcd for $C_{54}H_{72}N_6B_2F_8V$: C, 62.98; H, 7.05; N, 8.16; V, 4.95. Found: C, 63.11; H, 7.20; N, 7.95; V, 4.79.

[V(^{t}bpy)$_3$](BF$_4$)$_3$. A 20 mL scintillation vial charged with [V(^{t}bpy)$_3$] (60 mg; 0.07 mmol) dissolved in THF (10 mL) was treated portionwise with ferrocenium tetrafluoroborate (60 mg; 0.071 mmol) and stirred for 18 h. The resultant bright red solution was stripped dry under vacuum, and the solids were washed several times to remove ferrocene. A dark red powder was obtained after recrystallization from acetonitrile/diethyl ether at −35 °C. Yield: 71 mg (89%).

Anal. Calcd for $C_{54}H_{72}N_6B_3F_{12}V$: C, 58.09; H, 6.50; N, 7.53; V, 4.56. Found: C, 58.35; H, 6.64; N, 7.30; V, 4.43.

Physical Methods. Electronic absorption spectra were recorded on a Perkin-Elmer Lambda 19 double-beam spectrophotometer (300−2100 nm). Cyclic and square wave voltammograms were recorded with an EG&G potentiostat/galvanostat 273A. A three electrode cell was employed with a glassy carbon working electrode, a glassy carbon auxiliary electrode, and a Ag/$AgNO_3$ reference electrode (0.01 M $AgNO_3$ in CH_3CN), in dichloromethane solution containing 0.1 M $[N(n\text{-}Bu)_4]PF_6$ as supporting electrolyte. Ferrocene was added as an internal standard after completion of the measurements, and potentials are referenced versus the Fc^+/Fc couple. Variable temperature (4−290 K) magnetization data were recorded in a 1 T magnetic field on a MPMS Quantum Design SQUID magnetometer. The experimental data were corrected underlying diamagnetism using tabulated Pascal's constants. X-band EPR spectra were recorded on a Bruker ELEXSYS E500 spectrometer and simulated with XSophe distributed by Bruker Biospin GmbH[16] or ESim (Dr Eckhard Bill). V K-edge XAS data were measured at the Stanford Synchrotron Radiation Lightsource (SSRL) under ring conditions of 3.0 GeV and 200 mA on beamline 7-3. The experimental setup, sample preparation, and data analysis have been detailed previously.[17] Elemental analyses were performed by H. Kolbe at the Mikroanalytischen Labor in Mülheim an der Ruhr, Germany. Accurate microanalyses for [V(^{t}bpy)$_3$] and Na[V(^{t}bpy)$_3$] were compromised by loss of a ^{t}bpy ligand was the sample is heated prior to combustion. Moreover, Na[V(^{t}bpy)$_3$] is extremely sensitive, and any measurements that required it be in solution always gave unsatisfactory results, including NMR, mass spectrometry, and electronic absorption. However, magnetic susceptibility data are a measure of bulk purity, and the data recorded for all four samples are consistent with their formulation. The parameters retrieved from the fit are correlated with the proposed electronic structure and EPR data for the neutral and dication.

Calculations. All DFT calculations were performed with the ORCA program.[18] All complexes were optimized using the B3LYP functional.[19] The all-electron basis sets were those reported by Weigend and Ahlrichs.[20] Triple-ξ-quality basis sets with one set of the polarization functions (def2-TZVP) were used for the metal vanadium and the nitrogen atoms. The remaining atoms were described by slightly smaller polarized split-valence def2-SV(P) basis sets that are double-ξ quality in the valence region and contain a polarizing set of d functions on the non-hydrogen atoms. Auxiliary basis sets used to

dx.doi.org/10.1021/ic202711s | Inorg. Chem. 2012, 51, 3707−3717

expand the electron density in the calculations were chosen to match the orbital basis. The self-consistent field calculations were tightly converged (1×10^{-8} E_h in energy, 1×10^{-7} E_h in the density charge, and 1×10^{-7} in the maximum element of the DIIS[21] error vector). The geometry search for all complexes was carried out in redundant internal coordinates without imposing geometry constraints. The Conductor-like Screening Model (COSMO) was used in the calculation of all charged species with THF as the solvent.[22] Van der Waals forces (DFT-D3) were included in the geometry optimizations of all molecules.[23] The broken symmetry (BS) approach was used to describe the computational results for $[V(bpy)_3]^{1+/0/1-}$.[24] Corresponding[25] and canonical orbitals and density plots were obtained using Molekel.[26]

Time-dependent (TD)-DFT calculations of the V K-pre-edges were conducted as previously described.[17,27] For all complexes, a single point calculation on the optimized structure was performed with a fully uncontracted CP(PPP) basis set for vanadium.[28] The same basis sets as described previously were used for the other atoms. TD-DFT calculations were then performed allowing only for transitions from the vanadium 1s orbital.[17] Due to shortcomings in the ability of DFT to model potentials near the nucleus an empirical shift of +115.35 eV was applied to ease comparison with the experimental spectra. Plots were obtained using "orca_mapspc" with a line broadening of 1.2 eV.

RESULTS AND DISCUSSION

Syntheses and Characterization. The dark blue neutral vanadium species $[V(^t bpy)_3]$ was initially prepared in a manner similar to the reduction method employed by Quirk and Wilkinson.[4] Typical of a highly reduced, formally low-valent early metal complex, it rapidly undergoes oxidation when exposed to air or water. The remaining members of the electron transfer series were subsequently prepared from $[V(^t bpy)_3]$. Reduction of $[V(^t bpy)_3]$ with sodium naphthalenide in THF solution generated the highly sensitive dark brown $Na[V(^t bpy)_3]$ in good yield (85%). The bright green dicationic and red tricationic tris(di-*tert*-butylbipyridine)vanadium compounds, $[V(^t bpy)_3](BF_4)_2$ and $[V(^t bpy)_3](BF_4)_3$, were prepared by oxidation of $[V(^t bpy)_3]$ with tropylium tetrafluoroborate and ferrocenium tetrafluoroborate, respectively. While $[V(^t bpy)_3](BF_4)_2$ proved to be somewhat air-sensitive, $[V(^t bpy)_3](BF_4)_3$ was persistently stable when handled in air.

Attempts were made to prepare the tris(di-*tert*-butylbipyridine)vanadium monocation; however, this compound could not be isolated in pure form due to persistent disproportionation to neutral $[V(^t bpy)_3]$ and dicationic $[V(^t bpy)_3]^{2+}$. The tris(bipyridine)vanadium monocation has been previously reported;[6] however, problems with disproportionation were also observed for this complex in most solvents, and we have found that disproportionation is accelerated with ^{t}bpy.

In order to investigate the extent of the electron transfer series of vanadium complexes with the di-*tert*-butyl substituted bipyridine ligand, the cyclic (CV) and square wave voltammograms of $[V(^t bpy)_3]$ were recorded in THF solution containing 0.1 M $[N(n\text{-}Bu)_4]PF_6$ as the supporting electrolyte at ambient temperature (Figures 1 and S1, Supporting Information). Reduction potentials quoted versus the Fc^+/Fc couple are listed in Table 1. Overall, the series of tris(di-*tert*-butyl-bipyridine)-vanadium complexes are highly reduced, consistent with reactive nature of $[V(^t bpy)_3]^{1-}$ and $[V(^t bpy)_3]$, especially. The voltammogram exhibits a reversible one-electron reductive wave at −2.38 V followed by an irreversible one-electron reductive wave at −2.79 V. The reversible reduction corresponds to the 0/1− couple, and the irreversibility of the further reduction wave is consistent with the fact that there is

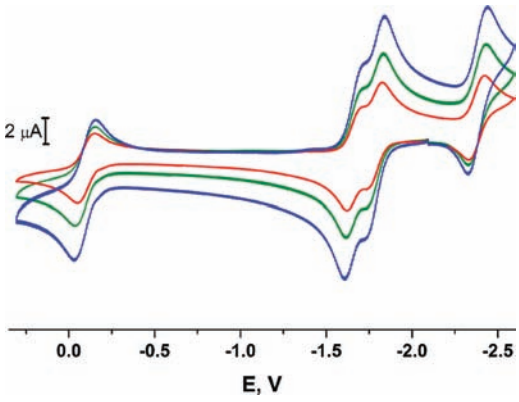

Figure 1. Cyclic voltammograms of $[V(^t bpy)_3]$ in THF solution (0.1 M $[N(n\text{-}Bu)_4]PF_6$ supporting electrolyte) at 25 °C with scan rates of 100, 200, and 400 mV s^{-1} (glassy carbon working electrode). Potentials are referenced versus the Fc^+/Fc couple.

no evidence for a dianionic species, nor a trianionic despite the reported isolation for $Na_3[V(bpy)]\cdot 7THF$.[12]

In addition, three reversible one-electron oxidative waves are observed at −1.78 V, −1.66 V, and −0.09 V, corresponding to the 1+/0, 2+/1+, and 3+/2+ couples, respectively. The square wave voltammogram also includes an irreversible oxidation at 0.80 V (Figure S1, Supporting Information). The proximity of the first and second oxidation waves, separated by 120 mV, and a small comproportionation constant (for the formation of a monocation) can be estimated from the difference between the 2+/1+ and 1+/0 couples to be K_c = 101,[29] underscoring the difficulty in isolating the monocationic species. The electrochemical data indicates that the tri- and dicationic species should be stable and isolable complexes, and this is indeed observed experimentally.

The difference in potential of more than 1 V between the redox events at −0.09 and −1.66 V suggests that oxidation from di- to trication is metal-based, resulting in a change of oxidation state at the from +II to +III. Likewise, the profoundly negative potentials of the 2+/1+ and 1+/0 couples is consistent with ligand-based reduction events leading to formulation of the neutral species as having two ligand radicals and maintaining a +II central ion.

The electronic spectra for the series of di-*tert*-butyl substituted vanadium complexes were also studied, and the data is summarized in Table 2. Electronic spectra have been previously recorded for the series of unsubstituted $[V(bpy)_3]^z$ complexes (z = 2+, 1+, 0, 1−); however, analysis of the corresponding trication $[V(bpy)_3]^{3+}$ is lacking.[9,30,31] Despite repeated attempts, the monoanion was too sensitive in dilute solution to survive data collection. For our series, similar features were observed between 13 000 and 30 000 cm^{-1} for all compounds (Figure 2). For $[V(^t bpy)_3]$ and $[V(^t bpy)_3]^{2+}$, the highest energy peak appears at ~24 000 cm^{-1}, while the highest energy peak for $[V(^t bpy)_3]^{3+}$ is shifted to 27 700 cm^{-1} (Table 2). For each compound, an additional peak at lower energy appears to be composed of several overlapping bands (Figure 2). On the basis of the intensity of these transitions and previous analysis of $[V(bpy)_3]^{2+}$ and $[V(bpy)_3]^0$,[31] we assign these features between 13 000 and 30 000 cm^{-1} as metal-to-ligand charge transfer (MLCT) bands for $[V(^t bpy)_3]$ and $[V(^t bpy)_3]^{2+}$. Likewise for $[V(^t bpy)_3]^{3+}$, the overlapping transitions centered around 20 000 cm^{-1} could be considered charge transfer bands to/from the metal.

dx.doi.org/10.1021/ic202711s | Inorg. Chem. 2012, 51, 3707−3717

Table 1. Redox Potentials[a] (V) for Complexes

	$E_{1/2}$ (4+/3+)	$E_{1/2}$ (3+/2+)	$E_{1/2}$ (2+/1+)	$E_{1/2}$ (1+/0)	$E_{1/2}$ (0/1−)	$E_{1/2}$ (1−/2−)	$E_{1/2}$ (1−/2−)
$[V(^t bpy)_3]^b$	0.80 irr[c]	−0.09	−1.66	−1.78	−2.38	−2.79 irr[c]	
$[V(bpy)_3]^d$			−1.41	−1.51	−2.05	−2.73	−3.13

[a]Referenced versus Fc^+/Fc. [b]Measured in THF. [c]irr = irreversible. [d]Recorded in DMF in ref 5.

Table 2. Electronic Absorption Data for Complexes

complex	λ_{max}, cm^{-1} (ε, 10^4 M^{-1} cm^{-1})
$[V(^t bpy)_3]$	23753 (0.39), 16639 (0.50), 9940 (0.39), 7194 (0.16)
$[V(^t bpy)_3]^{2+}$	23866 (0.30), 15129 (0.42)
$[V(^t bpy)_3]^{3+}$	27701 (0.72), 20704 (0.26), 18939 (0.30)

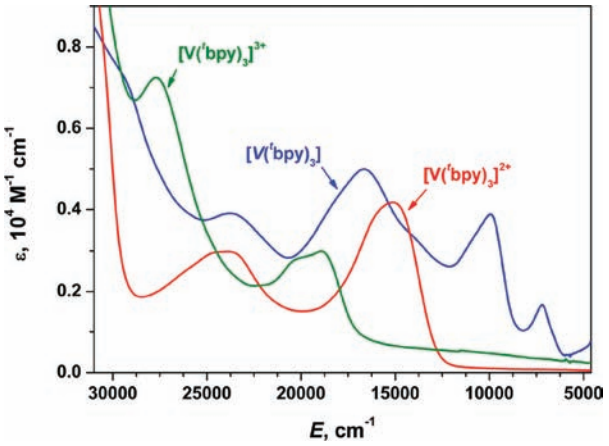

Figure 2. Electronic absorption spectra for $[V(^t bpy)_3]^z$ (z = 3+ (green), 2+ (red), 0 (blue)) recorded in THF at ambient temperature.

Additional features in the near-infrared (NIR) region are observed in the spectra of $[V(^t bpy)_3]^{1-}$ and $[V(^t bpy)_3]$, which are consistent with coordinated ligand radicals. For the latter, the feature at 9940 cm^{-1} (1006 nm) is clearly composed of several overlapping transitions, presumably MLCT or LMCT in nature. A much less intense band at 4460 cm^{-1} (2300 nm), which is more easily seen in the IR spectrum (Figure S2, Supporting Information), is considered an intervalence charge transfer (IVCT) transition diagnostic of ligand mixed-valency. Similar low energy transitions (4000−6000 cm^{-1}) have been observed for transition metal complexes with mixed-valent redox-active ligands,[32] most notably $[Ru(bpy)_3]^{1+}$ and $[Ru(bpy)_3]^0$, which exhibit a weak band at 4500 cm^{-1} consistent with their formulation as $[Ru^{II}(bpy^{\bullet})(bpy^0)_2]^{1+}$ and $[Ru^{II}(bpy^{\bullet})_2(bpy^0)]^0$, respectively.[33]

The solid state magnetic susceptibilities for the series of tris(di-*tert*-butylbipyridine)vanadium complexes were determined by magnetochemical measurements over the range 4−290 K. The results for all paramagnetic complexes are displayed in Figure 3; $Na[V(^t bpy)_3]$ was found to be diamagnetic (Figure S3, Supporting Information). Charge-neutral $[V(^t bpy)_3]$ displayed a temperature independent magnetic moment of 1.80 μ_B between 50 and 290 K for g = 1.985, establishing an $S = {}^1/_2$ ground state in accord with the assignment for $[V(bpy)_3]$.[31] The steep decline in magnetic moment < 50 K is due to weak intermolecular antiferromagnetic coupling and was successfully modeled by including a Weiss constant, θ_W = −8 K.

Dicationic $[V(^t bpy)_3]^{2+}$ exhibited an effective magnetic moment of 3.84 μ_B, consistent with three unpaired electrons and an $S = {}^3/_2$ ground state (Figure 3). Its magnetic behavior was virtually invariant over the entire range measured, and the

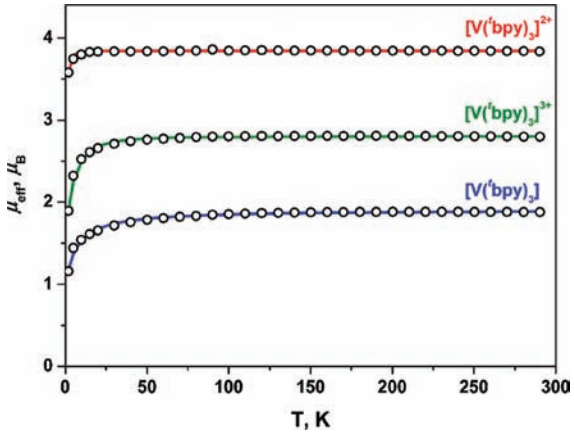

Figure 3. Temperature dependence of the magnetic moment, μ_{eff}, μ_B, of powder samples of $[V(^t bpy)_3]$ (blue), $[V(^t bpy)_3](BF_4)_2$ (red), and $[V(^t bpy)_3](BF_4)_3$ (green) at 1 T. Circles represent experimental data, and solid lines represent simulations.

miniscule decline in the response below 20 K is indicative of a small zero-field splitting parameter (D) synonymous with a $(t_{2g})^3$ central ion. The data was successfully modeled with g = 1.97, D = −0.57 cm^{-1}, and rhombicity, E/D = 0.09, fixed from EPR (vide infra). The magnetism of $[V(^t bpy)_3]^{3+}$ is attended by an effective magnetic moment of 2.80 μ_B between 50 and 290 K, with a pronounced decrease in the magnetic moment below 50 K (Figure 3), establishing an S = 1 ground state. The low temperature part of the spectrum was modeled with a large zero-field splitting of $|D|$ = 20.4 cm^{-1} and an E/D = 0.05. The magnitude of D stems from the ease in which valence e electrons can be promoted into the nearby a_1 orbital by spin−orbit coupling,[34] a mechanism unavailable to the V(II) ion in $[V(^t bpy)_3]^{2+}$.

With the spin ground states of the tris(di-*tert*-butylbipyridine)vanadium complexes established, EPR spectroscopy was used to further probe the electronic structures. The EPR spectrum of $[V(bpy)_3]$ has been previously recorded both in fluid and in frozen solution. The earliest measured fluid solution spectrum was by Elschner and Herzog at 293 K.[10] This result was replicated independently by König[7] and Davison et al.,[8] where both the ^{51}V ($I = {}^7/_2$, 99.75% abundant) and ^{14}N (I = 1, 99.63% abundant) hyperfine coupling constants of 77.3 × 10^{-4} cm^{-1} and 2.1 × 10^{-4} cm^{-1}, respectively, were observed. The frozen solution spectrum was first reported by Rieger et al. and diagnosed with nearly isotropic g-values and an axial ^{51}V hyperfine coupling ($A_\perp$ = 86 × 10^{-4} cm^{-1}; $A_\parallel$ = 48 × 10^{-4} cm^{-1}).[11] In all cases, the complex was described as having a V(0) center, with Davison et al. and Reiger et al. postulating that the SOMO of $[V(bpy)_3]$ is best described as highly delocalized into the bpy π^* system, with the latter deriving a 30% metal contribution to the magnetic orbital.

The EPR spectrum of $[V(^t bpy)_3]$ was recorded in both fluid (Figure S4, Supporting Information) and in frozen (Figure 4) solution; the simulation parameters are summarized in Table 3. The eight-line pattern in the fluid solution spectrum was

dx.doi.org/10.1021/ic202711s | Inorg. Chem. 2012, 51, 3707−3717

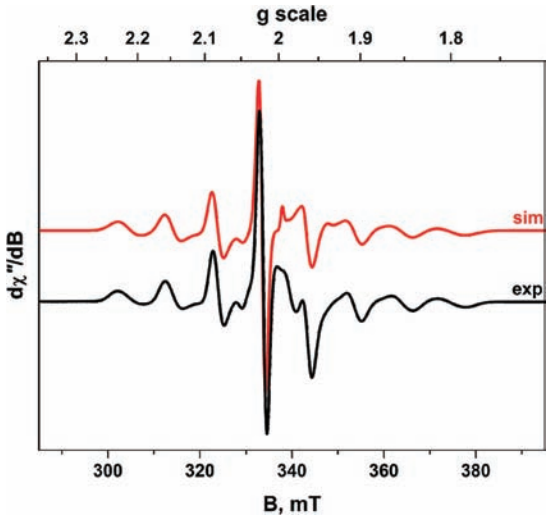

Figure 4. X-band EPR spectrum of $[V(^{t}bpy)_3]$ in THF recorded at 20 K (experimental conditions: frequency 9.4367 GHz; power 0.06 mW; modulation 0.5 mT). Experimental spectrum depicted in black and the simulation as a red line.

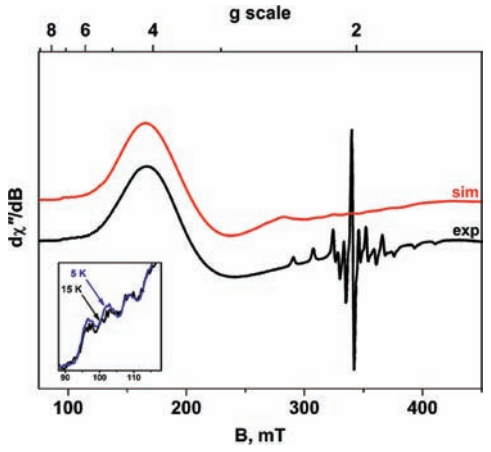

Figure 5. X-band EPR spectrum of $[V(^{t}bpy)_3]^{2+}$ in THF recorded at 15 K (experimental conditions: frequency 9.6309 GHz; power 0.63 mW; modulation 0.8 mT). Experimental spectrum is depicted by the black line, and the simulation is shown in red. Inset shows the intensity of the resolved feature at $g_{eff,z} \sim 6$ signal from the excited $m_s = \pm^3/_2$ Kramer's doublet. The marginally greater intensity in the 5 K spectrum indicates a negative zero-field splitting for this complex.

simulated with $g_{iso} = 1.985$ and $A_{iso} = 77.9 \times 10^{-4}$ cm^{-1} with an overall appearance consistent with a metal-based spin in a trigonal ligand field such as neutral and dianionic tris-(dithiolene) analogues (Table 3).[17] Here, the ^{51}V hyperfine interaction is much larger (~25%) because of reduced covalency in the V−N bonds compared with their V−S counterparts which concentrates more spin on the metal and concomitant with the larger computed metal character in this orbital (vide infra). No superhyperfine coupling to ^{14}N was observed. Moreover, the frozen solution spectrum is also very reminiscent of the tris(dithiolene) spectra with negligible anisotropy in the *g*-values but a large anisotropy in the axially split magnetic hyperfine interaction. This is the hallmark of a metal-based SOMO with a_1 symmetry that in essence describes the vanadium d_{z^2} orbital. The difference between $[V(^{t}bpy)_3]$ and its tris(dithiolene) analogues is seen in the anisotropy of the hyperfine coupling, with the former exhibiting a much larger $A_{||}$-value. This was noted by Rieger et al., and from this the metal content of the ground state was computed as ~30%.[11] The value is at odds with the other experimental and theoretical data included in this study (vide infra) where 90% metal character is found in the a_1 SOMO and can conceivably be attributed to the assumption in Reiger's calculation that this system is treated as $(d_{z^2})^1$, ignoring the other d orbital spins that comprise a high-spin V(II) ion.

The frozen solution EPR spectrum of $[V(^{t}bpy)_3]^{2+}$ shown in Figure 5 comprises an axial signal with effective *g*-values of ~4 and ~2 characteristic of an $S = {}^3/_2$ ground state with $|D| > h\nu$ (0.3 cm^{-1} at X-band). Additionally, there is a multiline feature at $g_{eff} \sim 6$ derived from the excited $m_s = \pm^3/_2$ Kramer's doublet whose intensity reflects the magnitude of *D* and can define its sign with measurement at two temperatures, at 5 and 15 K (Figure 5, inset). The spectrum was simulated with $g = (1.925, 1.925, 2.065)$, $A = (-107, -107, -165) \times 10^{-4}$ cm^{-1}, $D = -0.57$ cm^{-1}, and $E/D = 0.09$, with the experimental line width accommodated by a Gaussian distribution of E/D of $\sigma = 0.04$. The high field region of the spectrum is blighted by a multiline spectrum centered at $g \sim 2$ diagnostic of a vanadyl species (Figure S5, Supporting Information), which constitutes <1% of the signal intensity and stems from decomposition of $[V(^{t}bpy)_3]^{2+}$ by adventitious water and air. Although this obscures the $A_{||}$ lines, we could obtain a very accurate estimate from the eight-line splitting of the $g_{eff} \sim 6$—the parallel component of the $m_s = \pm^3/_2$ Kramer's doublet. Overall, this is the trademark signal of a high-spin V(II) d^3 central ion in $[V(^{t}bpy)_3]^{2+}$.

V K-edge X-ray absorption spectroscopy (XAS) is a proven means to directly evaluate the oxidation state of the vanadium ion. This is achieved essentially by locating the energies of both the pre- and rising-edge spectral features, which stem from electric quadrupole-allowed V 1s → 3d and electric dipole-allowed V 1s → *n*p, and contrasting these values with known standards or internally calibrating within a given electron transfer series. Furthermore, the intensity of pre-edge transitions have been shown to relate coordination geometry with the greater departure from centrosymmetry lending dipole character to the transition via an introduction of metal p character into the d orbitals.[17] The long core-hole lifetime

Table 3. Spin-Hamiltonian *g*- and *A*-Values[a] Derived from Spectral Simulation of Complexes

complex	g_{iso}	g_x	g_y	g_z	A_{iso}	A_{xx}	A_{yy}	A_{zz}
$[V(^{t}bpy)_3]$	1.985	1.981	1.982	1.993	−77.9	−96.3	−96.3	−41.0
$[V(bpy)_3]^b$	1.983	1.981	1.981	1.988	−73.5	−86.0	−86.0	−48.0
$[V(pdt)_3]^c$	1.991	1.989	1.991	1.993	−57.2	−83.0	−80.5	−5.0
$[V(^{t}bpy)_3]^{2+}$		1.925	1.925	2.065		−107	−107	−165

[a] In 10^{-4} cm^{-1}. The sign is assumed to be negative owing to the dominant Fermi contact contribution. [b] Reference 11. [c] Reference 17; pdt =1,2-diphenyl-1,2-dithiolate(2−).

dx.doi.org/10.1021/ic202711s | *Inorg. Chem.* 2012, 51, 3707−3717

observed with first-row transition metals leads to well-resolved pre- and rising-edge spectral components. The V K-edge spectra are shown in Figure 6 and the pre- and rising-edge energies are collected in Table 4.

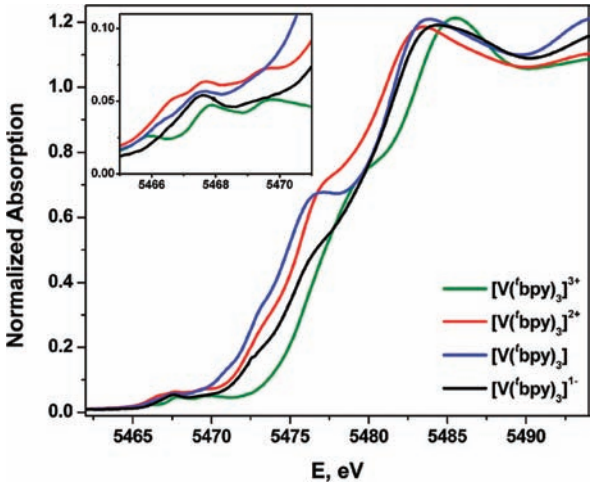

Figure 6. Comparison of normalized V K-edge XAS spectra for compounds $[V(^t bpy)_3]^z$ (z = 3+, 2+, 0, 1−). The inset shows an expansion of the pre-edge region.

Table 4. Experimental Pre- and Rising-Edge Energies (eV) for Complexes

complex	pre-edge	rising edge
$[V(^t bpy)_3]^{1-}$	5467.6	5475.0
$[V(^t bpy)_3]$	5467.5	5474.2
$[V(^t bpy)_3]^{2+}$	5466.7	5473.4
	5467.7	
	5469.5	
$[V(^t bpy)_3]^{3+}$	5466.0	5476.0
	5467.9	
	5469.7	

Glancing at the data shown in Figure 6, a swift diagnosis of the effective nuclear charge of the vanadium ion for each member of the series is not immediately apparent. Taking $[V(^t bpy)_3]^{2+}$ and $[V(^t bpy)_3]^{3+}$ since they are readily characterized as having three neutral ($^t bpy^0$) ligands coordinated to a V(II) and V(III) ion, respectively, there is a difference of 2.6 eV in their rising-edge energies concomitant with their different oxidation states. Although this is significantly greater than the general rule-of-thumb for XAS, that a ∼1 eV shift accounts for a change in the oxidation state by one unit, the rising-edge also comprises unresolved transitions to higher p states of the metal and low-lying predominantly ligand π^* states with some metal character and double quantum excitations. Moreover, the coordination geometry and ligand field strength will all contribute to the rising-edge profile and position. Therefore, it is often more beneficial to consult the pre-edge region since these are generally composed of one-electron transitions to vacant metal d orbitals. Nonetheless, it can also be seen that the rising-edge energies of $[V(^t bpy)_3]^{1-}$ and $[V(^t bpy)_3]$ are closer to that of the dication than the trication in accord with the premise that these both possess V(II) ions.

The pre-edge region for each compound is attended by a cluster of weakly intense peaks concominant with the near octahedral geometry calculated for this series (vide infra). However, one stand out observation is the clearly resolved low-energy feature at 5466 eV in the spectrum of $[V(^t bpy)_3]^{3+}$ that is 0.7 eV lower in energy than the first pre-edge feature—a shoulder—in the spectrum of $[V(^t bpy)_3]^{2+}$. As time-dependent (TD)-DFT calculations will demonstrate, this peak arises from a transition into the vacant a_1 orbital for the trication (vide infra); the same orbital is singly occupied in the V(II) ion. The more reduced members, $[V(^t bpy)_3]$ and $[V(^t bpy)_3]^{1-}$, also have a low-energy shoulder succeeded by two further peaks at similar energies, though their resolution is noticeably attenuated for the monoanion. Retrieving more critical details relies on the implementation of TD-DFT calculations to identify transitions contributing to the pre-edge peaks.

(a). Calculations. *Electronic Structures.* DFT calculations were carried out for the series of tris(bipyridine)vanadium complexes using the unsubstituted bpy ligand (sans ^{t}Bu groups). Geometry optimizations and ground state electronic structure calculations were performed using the B3LYP functional. Calculated metric parameters are listed in Table 5.

Tricationic $[V(bpy)_3]^{3+}$ was calculated using a spin-unrestricted Kohn−Sham (UKS) approach, with an S = 1

Table 5. Average Calculated Metric Parameters for Tris(bipyridine)vanadium Complexes

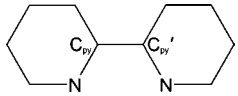

	$[V(bpy)_3]^{3-}$	$[V(bpy)_3]^{1-}$	$[V(bpy)_3]$	$[V(bpy)_3]^{1+}$	$[V(bpy)_3]^{2+}$	$[V(bpy)_3]^{3+}$
			bpy #1			
V−N (Å)	2.100	2.107	2.107	2.092	2.139	2.097
C_{py}−C_{py}' (Å)	1.428	1.417	1.438	1.433	1.475	1.471
C_{py}−N (Å)	1.394	1.393	1.378	1.382	1.355	1.359
			bpy #2			
V−N (Å)	2.140	2.106	2.107	2.124	2.140	2.097
C_{py}−C_{py}' (Å)	1.428	1.418	1.438	1.467	1.476	1.473
C_{py}−N (Å)	1.383	1.393	1.378	1.358	1.355	1.357
			bpy #3			
V−N (Å)	2.138	2.107	2.108	2.125	2.138	2.095
C_{py}−C_{py}' (Å)	1.427	1.417	1.438	1.468	1.477	1.473
C_{py}−N (Å)	1.384	1.392	1.378	1.358	1.355	1.358
twist angle (deg)	45.8	45.8	48.4	47.7	47.6	51.3

dx.doi.org/10.1021/ic202711s | Inorg. Chem. 2012, 51, 3707−3717

spin state based on the experimentally observed magnetic moment. The calculated intraligand bond distances are identical (Table 5). The average $C_{py}-C_{py}'$ distance of 1.472 Å and the average $C_{py}-N$ distance of 1.358 Å indicate three neutral ligands (bpy^0). The calculated geometry is nearly octahedral, with a twist angle of 51.3°. The observed deviation from ideal octahedral geometry (60°) is due to the constrained bite angle of the bpy ligand.

As expected for a tricationic complex with neutral (bpy^0) ligands, the calculated ground state comprises a high-spin V(III) center with two metal-based SOMOs (90%) of *e* symmetry (D_3 point group), essentially the $d_{x^2-y^2,xy}$ orbitals. The LUMO is also vanadium-centered (85%) and of a_1 symmetry (essentially d_{z^2}) and comprises a pseudo-$(t_{2g})^2$ set along with the SOMOs (Figure 7). A Mulliken spin population analysis

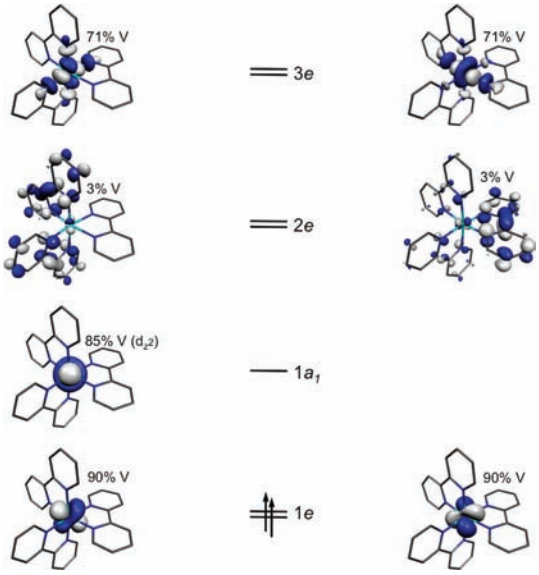

Figure 7. Qualitative MO manifold for $[V(bpy)_3]^{3+}$ derived from B3LYP DFT calculations.

sees two unpaired electrons (+2.11) deposited on the vanadium ion with negligible electron density on the ligands (Figure 8a). The empty $d_{xz,yz}$ orbitals (3*e*) are observed at much higher energy.

The tris(bipyridine)vanadium dication $[V(bpy)_3]^{2+}$ was calculated using an UKS approach as an $S = {}^3/_2$ species based on the experimentally observed magnetic moment. The metric parameters are consistent with neutral (bpy^0) ligands, with an average $C_{py}-C_{py}'$ distance of 1.476 Å and $C_{py}-N$ distance of 1.355 Å. The twist angle of 47.6° indicates a slightly greater deviation from ideal octahedral geometry than that observed with the trication, and a consequence of longer V−N bonds. Analysis of the MO manifold for $[V(bpy)_3]^{2+}$ demonstrates vanadium-centered SOMOs with virtually no involvement of the bpy ligands (Figure S6, Supporting Information). Due to the twist in this complex away from idealized octahedral geometry, the t_{2g} set is split into one *e* set and an a_1 orbital. The lower energy *e* orbitals are each singly occupied and consist of 77% vanadium character. The $1a_1$ orbital (87% V d_{z^2}) that comprised the LUMO of $[V(bpy)_3]^{3+}$ is now also singly occupied, giving rise to the overall spin-state of $S = {}^3/_2$. The LUMO and LUMO+1 of $[V(bpy)_3]^{2+}$ are primarily ligand-based orbitals of *e* symmetry. The Mulliken spin density plot for $[V(bpy)_3]^{2+}$ is also consistent with three unpaired electrons, with +2.91 spins located on the V ion and negligible spin density on the ligands (Figure 8b). Overall, the UKS solution for $[V(bpy)_3]^{2+}$ is consistent with a high-spin V(II) (d^3; $S = {}^3/_2$) complex with three (bpy^0) ligands.

Interestingly, the UKS calculation for the tris(bipyridine)-vanadium monocation, $[V(bpy)_3]^{1+}$, indicates a ligand-centered reduction of $[V(bpy)_3]^{2+}$. Spontaneous symmetry breaking into a broken symmetry BS(3,1) solution was observed with the UKS calculation. The distortion away from octahedral geometry (47.7°) results in a lower energy *e* set and an a_1 orbital, with a second empty 3*e* set higher in energy (Figure S7, Supporting Information). Three α-spins are observed at the vanadium center of $[V(bpy)_3]^{1+}$, occupying the same 1*e* set (75% V and 77% V) and $1a_1$ orbital (89% V d_{z^2}) observed for the dication. However, now a ligand-based *e* orbital is singly occupied, and strong antiferromagnetic coupling with the metal ion generates an $S = 1$ ground state. A coupling constant of $J = -610\ cm^{-1}$ was computed. The Mulliken spin density plot for $[V(bpy)_3]^{1+}$ also indicates three unpaired spins on the V ion (Figure 8c). The β-spin (−0.71) component is localized to one bpy ligand which reflects the calculated metric parameters where two ligands have bond lengths consistent with neutral (bpy^0) with the third ligand exhibiting a short $C_{py}-C_{py}'$ bond (1.433 Å) and elongated $C_{py}-N$ bonds (1.382 Å) affirming a monoanion π radical, $(bpy^{\bullet})^-$.

Unrestricted DFT calculations for the neutral tris-(bipyridine)vanadium complex indicates a further ligand-based reduction. Again, spontaneous symmetry breaking was observed with the UKS calculation for $[V(bpy)_3]$ giving an outcome identical to the BS(3,2) solution. However, in contrast to $[V(bpy)_3]^{1+}$, the ligand-based electron density of $[V(bpy)_3]$ is delocalized across all three ligands. The intraligand bond lengths are virtually identical between the three ligands, with an average $C_{py}-C_{py}'$ distance of 1.438 Å and an average $C_{py}-N$ distance of 1.378 Å. Although $[V(bpy)_3]$ has been previously crystallographically characterized,[13] comparison of the computed and experimental bond distances is dubious due to the

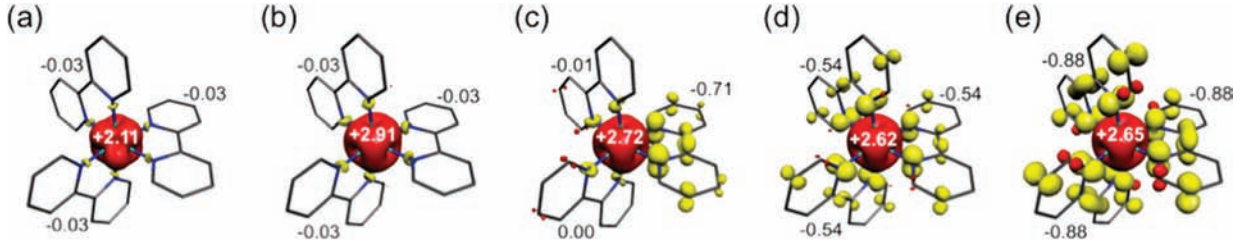

Figure 8. Mulliken spin population analyses for (a) $[V(bpy)_3]^{3+}$, (b) $[V(bpy)_3]^{2+}$, (c) $[V(bpy)_3]^{1+}$, (d) $[V(bpy)_3]$, and (e) $[V(bpy)_3]^{1-}$ (red: α-spin; yellow: β-spin).

dx.doi.org/10.1021/ic202711s | *Inorg. Chem.* 2012, 51, 3707−3717

limited structure resolution. Indeed, the crystal structure itself gives conflicting information about the extent of bpy ligand reduction, with long $C_{py}-C_{py}'$ bonds (avg. 1.468 Å) and also quite long $C_{py}-N$ bonds (avg. 1.406 Å). The twist angle of 48.4° indicates a distorted octahedron with D_3 symmetry, which is similar to the crystallographically measured twist angle of 53°. Analysis of the magnetic orbitals of $[V(bpy)_3]$ indicates three unpaired electrons on vanadium and two dispersed on all three ligands (Figure 8d). The SOMO is a metal-centered orbital (90% V d_{z^2}) of a_1 symmetry, consistent with EPR data (vide supra). The lower energy vanadium *e* orbitals, each with 74% vanadium character, couple to the ligand-based SOMOs, of equivalent symmetry, with integral overlap values of $S = 0.64$ consistent with strong antiferromagnetic coupling (Figure 9).

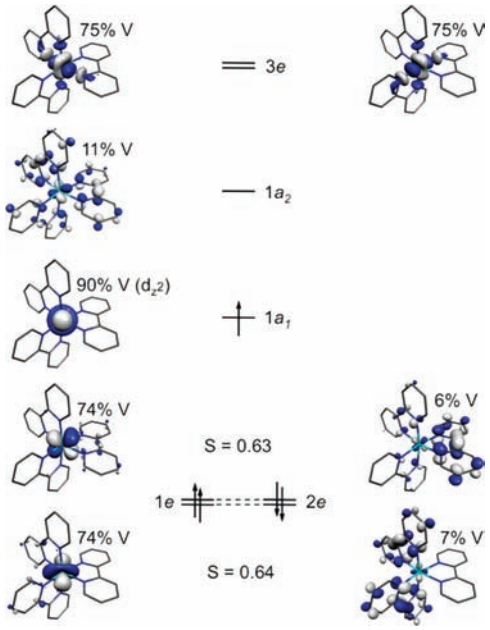

Figure 9. Qualitative MO diagram for $[V(bpy)_3]$ based on a BS(3,2) DFT calculation.

The computed coupling constant of $J = -651$ cm^{-1} highlights the strength of the interaction. The calculated spin densities support this electronic structure, with a positive electron density of +2.62 localized on the central metal atom and a negative electron density of −0.54 on each bpy ligand (Figure 8d). Therefore, the ground state electronic structure for $[V(bpy)_3]$ is best described as a high-spin V(II) ($S_V = {}^3/_2$) center antiferromagnetically coupled to two monoanionic ligand π radicals ($S_L = 1$) with a third neutral (bpy^0) ligand.

Diamagnetic $[V(bpy)_3]^{1-}$ was calculated using both spin-restricted and -unrestricted DFT approaches. The complex was calculated as a singlet based on the experimental magnetic data (Figure S3, Supporting Information). The UKS solution and the broken symmetry BS(3,3) solution were indistinguishable, with spontaneous symmetry breaking of the UKS solution. The resulting BS(3,3) solution was 28.9 kcal mol^{-1} more stable than the RKS solution, indicating that a simple closed-shell configuration is an inadequate description for this complex. The calculated metric parameters for $[V(bpy)_3]^{1-}$ indicate reduced bpy ligands, with shortened average $C_{py}-C_{py}$ bond distances of 1.417 Å and elongated average $C_{py}-N$ bond distances of 1.392 Å (Table 5). Analysis of the magnetic orbitals indicates three sets of antiferromagnetically coupled pairs (Figure S8, Supporting Information). Again, the twist angle of 45.8° results in splitting of the t_{2g} set into a lower energy *e* set and a higher energy a_1 orbital. The lower energy orbitals exhibit 73% vanadium character and comprise the 1*e* set. The corresponding β-spin orbitals are ligand-based with <5% vanadium character. The third α-spin represents the $1a_1$ orbital and is composed of 90% vanadium d_{z^2}, while its counterpart is exclusively ligand-based by virtue of its $1a_2$ symmetry, and hence the overlap value is extremely small ($S = 0.01$). On the basis of the calculated coupling constant of $J = -726$ cm^{-1}, the three ligands of $[V(bpy)_3]^{1-}$ are expected to be strongly coupled to the metal center. The spin density plot for $[V(bpy)_3]^{1-}$ shows +2.65 spins centered on the metal ion and −0.88 found on each ligand (Figure 8e) and leads to its formulation as $[V^{II}(bpy^{\bullet})_3]^{1-}$ ($S = 0$). This electronic structure is quite similar to that of the related $[Cr^{III}(^tbpy)_3]^0$ complex;[2] however, the calculated coupling constant for $[V(bpy)_3]^{1-}$ of $J = -726$ cm^{-1} is considerably larger than the value of $J = -477$ cm^{-1} calculated for the isolectronic Cr complex.

Herzog reported isolation of $Na_3[V(bpy)_3]\cdot 7THF$ and derived an $S = 1$ ground state based on room temperature magnetic measurements.[6] The computed electronic structure is most clearly expressed as a mixture of resonance structures $\{[V^{II}(bpy^{2-})_2(bpy^{\bullet})]^{3-} \leftrightarrow [V^{III}(bpy^{2-})_3]^{3-}\}$, as one of the metal SOMOs has approximately equivalent metal and ligand character and therefore a high integral overlap ($S = 0.90$) indicative of covalent bonding (Figure S9, Supporting Information). The Mulliken spin population analysis sees 2.42 spins at the metal and −0.42 dispersed unevenly over the bpy_3 unit; the covalency of the coupled pair attenuates the polarization such that these spin density values lie in between the V(II) and V(III) resonance forms (Figure S10, Supporting Information). The molecule has pseudo-C_3 symmetry quite unlike its isoelectronic Cr counterpart, $[Cr^{III}(bpy^{2-})_2(bpy^{\bullet})]^{2-}$.[2]

(b). Electronic Spectrum of [V(bpy)$_3$]. The electronic spectrum of $[V(bpy)_3]$ was calculated using time-dependent (TD)-DFT in an effort to assign the low-energy band observed in the electronic absorption and IR spectra. The spectrum was calculated using the B3LYP functional. Gratifyingly, TD-DFT calculations predict two transitions from the two ligand-based *e* orbitals corresponding to the bpy radical anions into the empty ligand-based $1a_2$ orbital corresponding to the third unreduced bpy ligand, characterized as an IVCT transition. These transitions are calculated at 4359 and 4369 cm^{-1}, in good agreement with the experimentally observed peak at ∼4500 cm^{-1} (Figure 10), and supports its assignment as an IVCT band. Moreover, such a peak was not observed in the experimental spectra of $[V(bpy)_3]^{2+}$ and $[V(bpy)_3]^{3+}$ and was also not predicted by TD-DFT calculations for these two compounds (Figures S11 and S12, Supporting Information).

(c). V K-Pre-Edge Spectra. The vanadium K-pre-edge X-ray absorption spectra for this series were explored using TD-DFT calculations with the B3LYP functional. This technique has previously been used successfully to study a series of related tris(dithiolene)vanadium complexes.[17] Because this computational method can accurately determine relative transition energies but not the absolute transition energies, an energy correction must be used; here a shift of +115.35 eV was applied to each calculated spectrum.

The calculated vanadium pre-edge spectra for the dication, neutral, and monoanion are in good agreement with the experimental data (Figure 11). The calculated pre-edge peaks

dx.doi.org/10.1021/ic202711s | *Inorg. Chem.* 2012, 51, 3707−3717

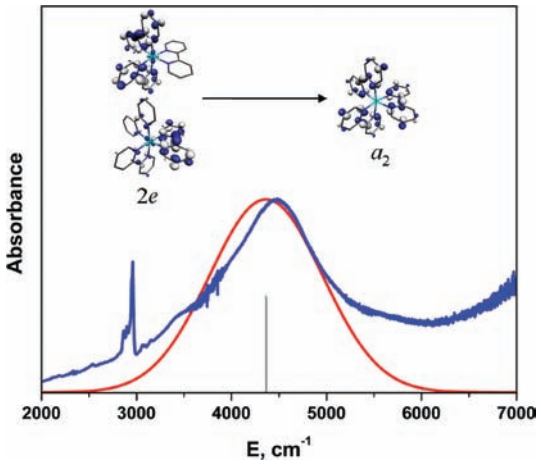

Figure 10. Calculated electronic spectrum (red) for $[V(bpy)_3]$ overlaid with experimental data (blue) for $[V(^tbpy)_3]$ of the IVCT transition. Stick plot denotes individual electronic transitions.

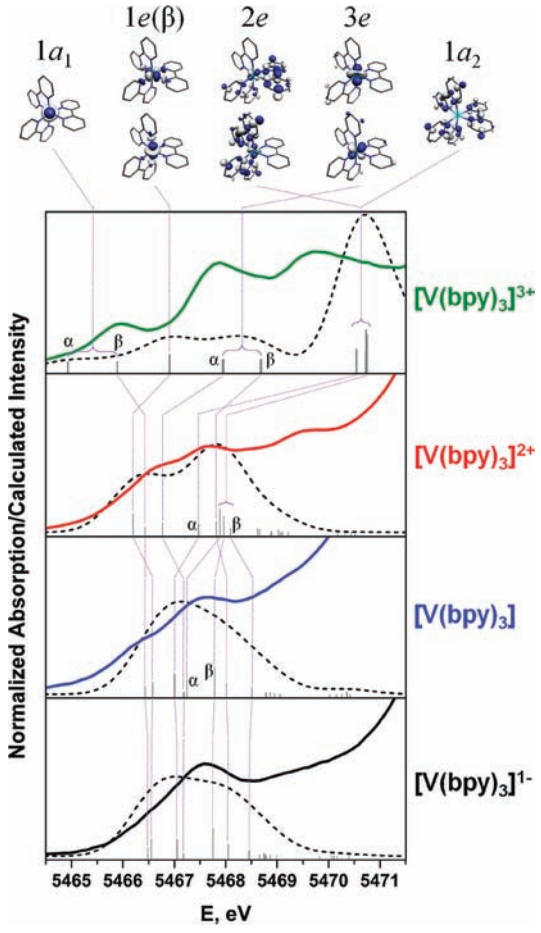

Figure 11. Comparison of experimental (solid line) and calculated (dashed line) V K-pre-edge spectra for $[V(bpy)_3]^{3+/2+/0/1-}$. Stick plots denote individual transitions from the orbitals identified above; α and β labels indicate spin-up and spin-down orbitals, respectively. Calculated intensity is in arbitrary units.

reveal that each is composed of several transitions, both to vanadium 3d orbitals and bpy π^* orbitals. In each case, the shift of the most intense experimental pre-edge peak matches well with the dipole-only bpy π^* 1a_2 transition, which is the most intense calculated transition due to symmetry-allowed mixing of V 4p$_z$ character (0.3−0.5%; Table S2, Supporting Information). A significant amount of 4p character is present in the V 1*e* and 3*e* MOs for the V(II) compounds, $[V(bpy)_3]^{2+/0/1-}$, due to d−p mixing (Table S2, Supporting Information). A much smaller amount of 4p character is generally observed for $[V(bpy)_3]^{3+}$ because of the large twist angle, and therein a more centrosymmetric species. Mixing of 4p character into the bpy π^* orbitals was also observed, although to a smaller extent than with the metal-based orbitals.

For complexes $[V(bpy)_3]^{2+/0/1-}$, the pre-edge region lies in the range 5466−5469 eV, consistent with having the same +II oxidation state, with little variation in the computed transition energies of their respective pre-edge regions. Recall that the electronic structure of $[V(bpy)_3]^{1-}$ is best described as having three singly occupied vanadium SOMOs antiferromagnetically coupled to three bpy π radical monoanions; as expected from this electronic structure, the pre-edge peak for $[V(bpy)_3]^{1-}$ arises mainly from transitions to the corresponding empty vanadium 1*e* and 1a_1 β-spin orbitals and bpy π^* α-spin orbitals (Figure 11). Additional transitions to the unoccupied vanadium 3*e* orbitals are also observed. Similarly, transitions to the same orbitals are observed for $[V(bpy)_3]$, with an additional transition to the now empty 1a_2(β) orbital (Figure 11). For $[V(bpy)_3]^{2+}$, where all ligands exist in their neutral form, transitions are observed to both α- and β-spin bpy π^* orbitals of *e* and a_2 symmetry.

Additional pre-edge transitions were calculated for the pre-edge spectrum of $[V(bpy)_3]^{3+}$ (Figure 11). Notably, the transition to the 1a_1(α) orbital is found to be ∼2 eV lower in energy than the corresponding transition for the other members of the series, and for this d^2 ion, significant polarization (∼1 eV) of the 1a_1 and 1*e* orbitals is observed. However, the lowest energy transition for $[V(bpy)_3]^{3+}$, to the unoccupied 1a_1(α) orbital, is only very faintly observed in the experimental spectrum due to the low intensity. The pronounced difference between the experimental and calculated pre-edge spectrum of $[V(bpy)_3]^{3+}$ stem from an overestimation of the spin polarization, and the input from several transitions to the pre-edge peaks undermine even a tentative assignment. The vanadium 1a_1(β) transition in $[V(bpy)_3]^{3+}$ is also found ∼1 eV lower in energy than for the other compounds. This is expected because the V(II) complexes all have singly occupied 1*e* and a_1 orbitals, while for $[V(bpy)_3]^{3+}$ the vanadium 1a_1 orbital is empty. In general, the pre-edge peaks for $[V(bpy)_3]^{3+}$ have a much lower intensity than those of $[V(bpy)_3]^{1-}$, $[V(bpy)_3]$, and $[V(bpy)_3]^{2+}$ because of attenuated 4p character modulated by the twist angle and greater polarization of the d orbitals.

CONCLUSIONS

The electronic structure of a series of di-*tert*-butyl substituted tris(bipyridine)vanadium complexes was examined through a combination of EPR spectroscopy, electronic absorption spectroscopy, cyclic voltammetry, solid state magnetometry, XAS, and (TD)-DFT calculations. From these studies, a clear picture regarding the electronic structure of these compounds has emerged. The tricationic complex, $[V^{III}(^tbpy^0)_3]^{3+}$, is best described as a high-spin V(III) (d^2; S_V = 1) ion complexed by three neutral ($^tbpy^0$) ligands. One-electron reduction to the dicationic complex, $[V^{II}(^tbpy^0)_3]^{2+}$, results in reduction of the metal center to give a d^3 high-spin V(II) metal center, again with three neutral ligands. Notably, the next three one-electron reductions are ligand-based, giving monocationic $[V^{II}(^tbpy^{\bullet})^-$

dx.doi.org/10.1021/ic202711s | *Inorg. Chem.* 2012, 51, 3707−3717

(^{t}bpy^0)$_2$]$^{1+}$, neutral [V^{II}(^{t}bpy$^•$)$_2$(^{t}bpy^0)]^0, and monoanionic [V^{II}(^{t}bpy$^•$)$_3$]$^{1-}$; the metal ion is invariantly +II. However, these complexes also possess one, two, and three monoanionic (^{t}bpy$^•$)$^-$ π radical ligands, respectively. DFT calculations suggest that the bpy ligands in [V^{II}(bpy$^•$)(bpy^0)$_2$]$^{1+}$ are class II mixed-valency (localized), whereas by virtue of the D_3 symmetry, they are class III (delocalized) in neutral [V(bpy$^•$)$_2$(bpy^0)]. The most reduced member of the series, only seen for the unsubstituted bpy ligand, is best described with resonance structures {[V^{II}(bpy^{2-})$_2$(bpy$^•$)]$^{3-}$ ↔ [V^{III}(bpy^{2-})$_3$]$^{3-}$}. This series of tris(bipyridine)vanadium compounds makes an interesting comparison with the related chromium series, where all reductions occur at the bpy ligands while maintaining V(II) and Cr(III) central ions, respectively, and further highlights the inherent stability of such high-spin d^3 ions in coordination complexes. However, unlike the rigid consistency of the +III ion for all homoleptic chromium complexes of this type, the exchange stabilization within the d^3 vanadium ion is not as potent, and therefore while a +II ion is observed for tris(bipyridine), a V(IV) ion is diagnosed in the analogous tris(dithiolene) series.[17] Moreover, neutral tris(dioxolene)vanadium was given a +III oxidation state based on IR data,[35] whereas the crystallographic parameters were more befitting a +V oxidation state.[36] The variation in vanadium oxidation states permits comparison of the different donor strengths and polarizability of the bidentate ligands. Such a contrast mandates an unambiguous description of the electronic structure for each series, therein underscoring the importance of the combined multispectral and theoretical approach to meet this realization in these simple molecules that have relevance to more elaborate chemical systems.

■ ASSOCIATED CONTENT

Ⓢ Supporting Information

Square-wave voltammogram and IR spectrum of [V(^{t}bpy)$_3$]; magnetic susceptibility data for Na[V(^{t}bpy)$_3$]; EPR spectra of [V(^{t}bpy)$_3$] and oxovanadium impurity in [V(^{t}bpy)$_3$]$^{2+}$. Tables of calculated geometric and electronic structures details (qualitative MO schemes and Mulliken spin density plots) and TD-DFT calculated electronic spectra. This material is available free of charge via the Internet at http://pubs.acs.org.

■ AUTHOR INFORMATION

Corresponding Author

*E-mail: sproules@mpi-muelheim.mpg.de; wieghardt@mpi-muelheim.mpg.de.

Present Address

‡Department of Chemistry & Biochemistry, Colorado College, 14 E. Cache La Poudre, Colorado Springs, CO 80903, United States.

Notes

The authors declare no competing financial interest.

■ ACKNOWLEDGMENTS

A.C.B. and S.S. thank the Max-Planck-Society for a postdoctoral fellowship. SSRL operations are funded by the Department of Energy, Office of Basic Energy Sciences. The Structural Molecular Biology program is supported by the National Institutes of Health, National Center for Research Resources, Biomedical Technology Program, and by the Department of Energy, Office of Biological Environmental Research.

■ REFERENCES

(1) (a) Constable, E. C. *Adv. Inorg. Chem.* **1989**, *34*, 1. (b) Irwin, M.; Jenkens, R. K.; Denning, M. S.; Krämer, T.; Grandjeau, F.; Long, G. J.; Herdial, R.; McGrady, J. E.; Goicoechea, J. M. *Inorg. Chem.* **2010**, *49*, 6160. (c) Kraft, S. J.; Fanwick, P. E.; Bart, S. C. *Inorg. Chem.* **2010**, *49*, 1103. (d) Williams, B. N.; Huang, W.; Miller, K. L.; Diaconescu, P. L. *Inorg. Chem.* **2010**, *49*, 11493.

(2) Scarborough, C. C.; Sproules, S.; Weyhermüller, T.; DeBeer, S.; Wieghardt, K. *Inorg. Chem.* **2011**, *50*, 12446.

(3) (a) Behrens, H.; Müller, A. *Z. Anorg. Allg. Chem.* **1965**, *341*, 124. (b) Hein, F.; Herzog, S. *Z. Anorg. Allg. Chem.* **1952**, *267*, 337. (c) Herzog, S.; Grimm, U.; Waicenbauer, W. *Z. Chem.* **1967**, *7*, 355. (d) Herzog, S.; Renner, K. C.; Schön, W. *Z. Naturforsch.* **1957**, *12b*, 809.

(4) Quirk, J.; Wilkinson, G. *Polyhedron* **1982**, *1*, 209.

(5) Saji, T.; Aoyagui, S. *J. Electroanal. Chem.* **1975**, *63*, 405.

(6) Herzog, S. *Z. Anorg. Allg. Chem.* **1958**, *294*, 155.

(7) König, E. *Z. Naturforsch.* **1964**, *19a*, 1139.

(8) Davison, A.; Edelstein, N.; Holm, R. H.; Maki, A. H. *Inorg. Chem.* **1965**, *4*, 55.

(9) Hanazaki, I.; Nagakura, S. *Bull. Chem. Soc. Jpn.* **1971**, *44*, 2312.

(10) Elschner, B.; Herzog, S. *Arch. Sci.* **1958**, *11*, 160.

(11) Rieger, A. L.; Scott, J. L.; Rieger, P. H. *Inorg. Chem.* **1994**, *33*, 621.

(12) Herzog, S.; Grimm, U. *Z. Chem.* **1967**, *7*, 432.

(13) Albrecht, G. *Z. Chem.* **1963**, *3*, 182.

(14) (a) Breu, J.; Zwicknagel, A. *Z. Naturforsch., B: Chem. Sci.* **2004**, *59*, 1015. (b) Goodwin, K. V.; Pennington, W. T.; Petersen, J. D. *Inorg. Chem.* **1989**, *28*, 2016. (c) Hauser, A.; Maeder, M.; Robinson, W. T.; Murugesan, R.; Ferguson, J. *Inorg. Chem.* **1987**, *26*, 1331.

(15) Armarego, W. L.; Perrin, D. D. *Purification of Laboratory Chemicals*; Butterworth-Heinemann: Linacre House, Jordan Hill, Oxford, U.K., 2000.

(16) Hanson, G. R.; Gates, K. E.; Noble, C. J.; Griffin, M.; Mitchell, A.; Benson, S. *J. Inorg. Biochem.* **2004**, *98*, 903.

(17) Sproules, S.; Weyhermüller, T.; DeBeer, S.; Wieghardt, K. *Inorg. Chem.* **2010**, *49*, 5241.

(18) Neese, F. *Orca, an Ab Initio, Density Functional and Semiempirical Electronic Structure Program Package*, version 2.8; Universität Bonn: Bonn, Germany, 2010.

(19) (a) Becke, A. D. *J. Chem. Phys.* **1993**, *98*, 5648. (b) Lee, C. T.; Yang, W. T.; Parr, R. G. *Phys. Rev. B* **1988**, *37*, 785.

(20) Weigend, F.; Ahlrichs, R. *Phys. Chem. Chem. Phys.* **2005**, *7*, 3297.

(21) (a) Pulay, P. *Chem. Phys. Lett.* **1980**, *73*, 393. (b) Pulay, P. *J. Comput. Chem.* **1982**, *3*, 556.

(22) Klamt, A.; Schüürmann, G. *J. Chem. Soc., Perkin Trans. 2* **1993**, 799.

(23) Grimme, S.; Antony, J.; Ehrlich, S.; Krieg, H. *J. Chem. Phys.* **2010**, *132*, 154104.

(24) (a) Noodleman, L. *J. Chem. Phys.* **1981**, *74*, 5737. (b) Noodleman, L.; Case, D. A.; Aizman, A. *J. Am. Chem. Soc.* **1988**, *110*, 1001. (c) Noodleman, L.; Davidson, E. R. *Chem. Phys.* **1986**, *109*, 131. (d) Noodleman, L.; Norman, J. G.; Osborne, J. H.; Aizman, A.; Case, D. A. *J. Am. Chem. Soc.* **1985**, *107*, 3418. (e) Noodleman, L.; Peng, C. Y.; Case, D. A.; Monesca, J. M. *Coord. Chem. Rev.* **1995**, *144*, 199.

(25) Neese, F. *J. Phys. Chem. Solids* **2004**, *65*, 781.

(26) *Molekel*, Advanced Interactive 3D-Graphics for Molecular Sciences, Swiss National Supercomputing Center. http://www.cscs.ch/molkel.

(27) DeBeer George, S.; Petrenko, T.; Neese, F. *J. Phys. Chem. A* **2008**, *112*, 12936.

(28) Neese, F. *Inorg. Chim. Acta* **2002**, *337*, 181.

(29) Richardson, D. E.; Taube, H. *Inorg. Chem.* **1981**, *20*, 1278.

(30) (a) Fujita, I.; Yazaki, T.; Torii, Y.; Kobayashi, H. *Bull. Chem. Soc. Jpn.* **1972**, *45*, 2156. (b) Kaizu, Y.; Yazaki, T.; Torii, Y.; Kobayashi, H. *Bull. Chem. Soc. Jpn.* **1970**, *43*, 2068.

(31) König, E.; Herzog, S. *J. Inorg. Nucl. Chem.* **1970**, *32*, 601.

(32) (a) Banerjee, P.; Sproules, S.; Weyhermüller, T.; DeBeer George, S.; Wieghardt, K. *Inorg. Chem.* **2009**, *48*, 5829. (b) Chang, H.-

C.; Miyasaka, H.; Kitagawa, S. *Inorg. Chem.* **2001**, *40*, 146. (c) Kapre, R. R.; Bothe, E.; Weyhermüller, T.; DeBeer George, S.; Muresan, N.; Wieghardt, K. *Inorg. Chem.* **2007**, *46*, 7827.
(33) Heath, G. A.; Yellowlees, L. J.; Braterman, P. S. *Chem. Phys. Lett.* **1982**, *92*, 646.
(34) Palmer, G. In *Physical Methods in Bioinorganic Chemistry*; Que, J. L., Ed.; University Science Books: Sausalito, CA, 2000.
(35) (a) Cass, M. E.; Gordon, N. R.; Pierpont, C. G. *Inorg. Chem.* **1986**, *25*, 3962. (b) Simpson, C. L.; Pierpont, C. G. *Inorg. Chem.* **1992**, *31*, 4308.
(36) (a) Morris, A. M.; Pierpont, C. G.; Fenske, R. G. *Inorg. Chem.* **2009**, *48*, 3496. (b) Pierpont, C. G. *Inorg. Chem.* **2011**, *50*, 9766.